Organ-specificity of sterol and triterpene accumulation in *Arabidopsis thaliana*

B. Markus Lange[1,*], Brenton C. Poirier[1,3], Iris Lange[1], Richard Schumaker[1,4], and Rigoberto Rios-Estepa[2]

[1] Institute of Biological Chemistry and M.J. Murdock Metabolomics Laboratory, Washington State University, PO Box 646340, Pullman, WA 99164-6340, USA

[2] Grupo de Bioprocesos, Departamento de Ingeniería Química, Universidad de Antioquia, Calle 70 No. 52-21, Medellín, Colombia

[3] Current address: Elo Life Sciences, 5 Laboratory Drive, Research Triangle Park, NC 27709, USA

[4] Current address: Alma Rosa Winery, 180-C Industrial Way, Buellton, CA 93427, USA

*** Corresponding author:**
B. M. Lange, Institute of Biological Chemistry and M.J. Murdock Metabolomics Laboratory, Washington State University, PO Box 646340, Pullman, WA 99164-6340, USA; Tel.: 509-335-3794; Fax: 509-335-7643; e-Mail: lange-m@wsu.edu

Running title:
Arabidopsis sterols and triterpenes

Keywords:
Arabidopsis; kinetic mathematical model; metabolic engineering; sterol; triterpene

ABSTRACT

Sterols serve essential functions as membrane constituents and hormones (brassinosteroids) in plants, while non-sterol triterpenoids have been implicated in defense responses. Surprisingly little is known about the sterol and triterpene profiles in different plant organs. To enhance our understanding of organ-specific sterol and triterpene accumulation, we quantified these metabolite classes in four different organs (root, stem, leaf, seed) of *Arabidopsis thaliana* (L.). Based on these data sets we developed kinetic mathematical models of sterol biosynthesis to capture flux distribution and pathway regulation in different organs. Simulations indicated that an increased flux through the sterol pathway would not only result in an increase of sterol end products but also a concomitant build-up of certain intermediates. These computational predictions turner out to be consistent with experimental data obtained with transgenic plants ectopically overexpressing 3-hydroxy-3-methylglutary-coenzyme A reductase (*HMG1* gene). The opportunities and limitations of incorporating mathematical modeling into the design of approaches to engineer sterol biosynthesis are discussed.

INTRODUCTION

Free sterols, sterol glycosides and acyl sterol glycosides are major lipid constituents of the plasma membrane (PM) in plants, accounting for > 40 mol-% of the total lipids within the PM of Arabidopsis (Uemura et al., 1995). Sterols are also enriched within detergent-resistant microdomains (DRMs) within the PM that are enriched in saturated fatty acids, sphingolipids and sterols, thus making them less fluid than the surrounding lipid bilayer (Georg et al., 2005; Takahashi et al., 2016). These regions serve as specific docking sites for proteins involved in cellulose synthesis (Bessueille et al., 2009), cold acclimation (Minami et al., 2015) and auxin transport (Willemsen et al., 2003). Mutation of sterol C-24 methyltransferase (SMT1) and experiments with methyl-β-cyclodextrin, a reagent that extracts sterols from membranes, have demonstrated that sterol depletion compromises the integrity of DRMs, thereby leading to the de-localization of DRM-associated proteins (Men et al., 2008; Kierszniowska et al., 2009). Sterols are also involved in several aspects of plant development, including male gametophyte and seed development (Jiang and Lin, 2013), embryo development, meristem function, hypocotyl elongation (Jang et al., 2000), stomatal development (Qian et al., 2013) and polar auxin transport (Willemsen et al., 2003; Men et al., 2008).

The biosynthesis of plant sterols has been the subject of a large number of studies, while the regulation of the pathway is much less understood. The mevalonate (MVA) pathway, which provides the bulk of precursors for the synthesis of sterols in plants, consists of eight enzymatic steps, yielding isopentenyl diphosphate (IPP) and dimethylallyl diphosphate (DMAPP) from acetyl-CoA (Hemmerlin et al., 2012) (Figure 1). One molecule of DMAPP and two molecules of IPP are then used to synthesize farnesyl diphosphate (FPP), which is further converted to squalene by squalene synthase (Kribii et al., 1997; Busquets et al, 2008). Squalene epoxidase generates squalene epoxide, which is the substrate for several triterpene synthases (Rasbery et al., 2007). The majority of squalene epoxide in leaves is usually converted to cycloartenol (> 85 % of all carbon produced by the MVA pathway), in the first committed step of the core sterol pathway (Babichuk et al., 2008). In the major route toward sterol synthesis in plants, the side chain of cycloartenol is methylated in a reaction catalyzed by SMT1 (Shi et al., 1996; Bouvier-Navé et al., 1997; Diener et al., 2000; Nes et al., 2003), and the sterol nucleus is subsequently modified. A minor route for sterol synthesis modifies cycloartenol to give cholesterol (Figure 1). The enzymes involved in further reshaping the sterol nucleus use products of both the cholesterol and cycloartenol methylation pathways as substrates. The downstream reactions involve a sterol demethylase complex (Pascal et al., 1993; Rondet et al., 1999; Darnet et al, 2001; Darnet and Rahier, 2004; Rahier et al., 2006; d'Andréa et al., 2007; Li et al., 2007; Rahier, 2011), an isomerization (Rahier et al., 1989; Lovato et al., 2000), a second demethylation (Taton and Rahier, 1991a; Kushiro et al. 2001; Kim et al., 2005), a double bond reduction (Taton et al., 1989; Schrick et al., 2000; Jang et al., 2000), and a second isomerization (Grebenok et al., 2000; Souter et al., 2002). At the following branch point, 4α-methyl-5α-cholest-7-en-3β-ol and 24-methylenelophenol can be converted, via a series of reactions, to cholesterol and campesterol, respectively. Alternatively, 24-methylenelophenol can undergo a second methylation of the side chain to yield 24-ethylidenelophenol, catalyzed by a second sterol C-24 methyltransferase (SMT2) (Shi et al., 1996; Husselstein et al., 1996; Zhou et al., 2003). Enzymes involved in the late

steps of sterol biosynthesis appear to operate on all three branches. These reactions involve a second sterol demethylase complex (Pascal et al., 1993; Rondet et al., 1999; Darnet et al, 2001; Darnet and Rahier, 2004; Rahier et al., 2006; d'Andréa et al., 2007; Li et al., 2007), a sterol desaturase (Gachotte et al., 1996; Taton and Rahier, 1996; Husselstein et al., 1999; Choe et al., 1999a), and two sterol reductases (Taton and Rahier, 1991b; Lecain et al., 1996; Klahre et al., 1998; Choe et al., 1999b; Choe et al., 2000), thereby leading to the major end products of the three branches, cholesterol, campesterol and β-sitosterol. Monooxygenases of the CYP710A family catalyze desaturations that generate the minor end products crinosterol/brassicasterol and stigmasterol (Morikawa et al., 2006; Arnqvist et al., 2008) (Figure 1).

Past studies on sterol accumulation have typically focused on a single organ or tissue cultured cells for analysis, but did not report on organ-specific compositional differences (Moreau et al., 2018). In the present study, we quantified sterols in four organs (root, stem, leaf, seed) of *Arabidopsis thaliana* (L.). Based on these data sets we developed kinetic mathematical models of sterol biosynthesis to capture flux distribution and pathway regulation in different organs. Simulations indicated that an increased flux through the sterol pathway would not only result in an increase of sterol end products but also a concomitant build-up of certain intermediates. These computational predictions were consistent with experimental data obtained with transgenic plants ectopically overexpressing 3-hydroxy-3-methylglutary-coenzyme A reductase (*HMG1* gene). The opportunities and limitations of incorporating mathematical modeling into the design of approaches to engineer sterol biosynthesis are discussed.

RESULTS AND DISCUSSION

Sterol profiles differ significantly across organs

Tissue samples were harvested at defined stages of Arabidopsis development (see Materials and Methods for details). In roots, the concentration of total sterols was 0.6 micromoles per gram fresh weight (µmol · g FW^{-1}) (Table 1). β-Sitosterol (49.6%), stigmasterol (22.5%) and campesterol (19.9%) were the major constituents, with cholesterol (1.3%), sterol pathway intermediates (total of 6.7 %; cycloartenol being the most abundant at 5.1%), and off-pathway triterpenoids (β-amyrin at 2.3% and lupeol at 0.4%) accumulating at lower levels (Table 1). Total sterols amounted to 0.4 µmol · g FW^{-1} in rosette leaves (Table 1). The major constituents were β-sitosterol (72.8%) and campesterol (17.0%), but sterol pathway intermediates (isofucosterol at 5.3% and cycloartenol at 4.5%) were also detected with considerable abundance. The total sterol level in Arabidopsis stems was 0.99 µmol · g FW^{-1}. β-Sitosterol (66.9%), campesterol (14.7%) and brassicasterol (9.2%) were highly abundant, while cholesterol (2.2%), sterol pathway intermediates (cycloartenol at 6.5%), and off-pathway triterpenoids (β-amyrin at 5.3%) were minor contributors to the sterol profile. Arabidopsis seeds had the highest total sterol content of the investigated samples (8.2 µmol · g FW^{-1}) (Table 1). Of the sterol pathway end products, β-sitosterol (71.2%) and campesterol (16.1%) were major constituents, with cholesterol (3.4%), stigmasterol (1.3%) and brassicasterol (1.0%) being minor contributors to the profile. The amounts of sterol pathway

intermediates (isofucosterol at 3.8% and cycloartenol at 2.6%) and off-pathway triterpenoids (β-amyrin at 1.9% and lupeol at 0.2%) were comparatively low (Table 1).

The information regarding sterol profiles in the literature is fragmentary, as most publications focus on a single organ. Roots were reported to contain high concentrations of β-sitosterol (70-80%), medium-high quantities of campesterol and stigmasterol (14-18 and 10-20%, respectively), and a relatively low cholesterol content (2-12%) (Wewer et al., 2011), which is generally consistent with our data, although the β-sitosterol content in our assays was significantly lower (50%). For stems and leaves, the reported composition is also in good agreement with our measurements (60-80% β-sitosterol, 14-18% campesterol, 0.5-2.0% cholesterol, and 0.5 - 1.0% stigmasterol) (Patterson et al., 1993; Gachotte et al., 1995; Schrick et al., 2000). High β-sitosterol amounts (75-80%) and medium-high quantities of campesterol (12-17%) were determined for seeds (stigmasterol and cholesterol levels not reported) (Chen et al., 2007), once again concurring with our data. The triterpenoids β-amyrin and lupeol were present in low quantities in most samples but, in stems, β-amyrin contributed more significantly (5% of total sterols and triterpenoids), which is consistent with other work on triterpenoids (Shan et al., 2008). To the best of our knowledge, the measurements presented here constitute the first data set directly comparing sterol and triterpenoid profiles across multiple organs, with the additional advantage of being obtained with a single analytical platform.

Kinetic mathematical models of Arabidopsis sterol biosynthesis predict accumulation of pathway intermediates in transgenic plants with increased precursor availability

The pathway scheme shown in Figure 1 served as the conceptual foundation to develop proof-of-concept-level kinetic mathematical models of sterol biosynthesis in Arabidopsis. As a first step, the available information regarding kinetic constants and other biochemical knowledge (such as inhibition or activation) was assembled from the literature (Table 2). The Michaelis constant (K_M) had been determined experimentally for many of the relevant enzymes but the turnover number (k_{cat}) had to be estimated in many cases. For these approximate calculations, the reaction rate (V_{max}) was taken into account when available ($k_{cat} = V_{max} / [E]$) (Table 2).

As a second step, rate equations were generated based on the Michaelis-Menten kinetics. For example, the change in the pool size of squalene (sterol biosynthesis intermediate) is determined by the rates of formation (v_1) and turnover (v_2) and can be expressed as follows:

$$\frac{\mathbf{d[Squalene]}}{\mathbf{dt}} = \mathbf{v_{1\,(SQS)}} - \mathbf{v_{2\,(SQE)}} = \frac{\mathbf{K_{kat(SQS)}\ [SQS]\ [FPP]}}{\mathbf{[FPP] + K_{m(SQS)}}} - \frac{\mathbf{K_{kat(SQS)}\ [SQE]\ [Squalene]}}{\mathbf{[Squalene] + K_{m(SQE)}}} \quad ;$$

with FPP, farnesyl diphosphate; SQE, squalene epoxidase; SQS, squalene synthase.

This formalism was used for the description of a total of 27 enzymatic reactions, with appropriate equations for unidirectional and reversible reactions, multi-substrate reactions (e.g.,

ternary complex or ping-pong mechanisms), and, if known, feedback inhibition. Numerical solutions for the resulting system of ordinary differential equations (ODEs) were calculated by an iterative process of approximation and error correction (MATLAB software package, MathWorks).

As a third step, the concentration of each enzyme in each of the five organs of interest had to be estimated. The ideal - but unfortunately too costly - approach would have been organ-specific quantitative proteomics data. We decided to infer enzyme concentrations from gene expression data instead, which, based on our previous work (Rios-Estepa et al., 2010; Lange and Rios-Estepa, 2014), can be employed as a first approximation. The organ-specific gene expression data sets employed in the current work had been made available as part of a prior publication (Schmid et al., 2005). The factor to convert gene expression levels (unitless) to enzyme concentrations (in µM) was determined by evaluating computationally which combination of values predicted sterol concentrations most closely matching those determined experimentally (a conversion factor of 6,800 was chosen) (Table 3).

As a fourth step, model adjustments were made to reflect an additional consideration. A factor (termed Kc40) was introduced to account for the esterification of sterol pathway end products (β-sitosterol, stigmasterol, campesterol and cholesterol) and/or incorporation into biological membranes, which reduces the concentration of free sterols and thereby the potential for acting as feedback inhibitors of other biosynthetic enzymes (in particular sterol methyltransferases). Simulations were performed assuming a 50 d (7 week) growth period. The full details of the computational approaches used in this study are available in Supplemental Methods and Data File S1).

Our model for root sterol accumulation predicted high β-sitosterol levels (0.29 µmol · g FW^{-1}) and relatively low concentrations for campesterol and stigmasterol (0.05 and 0.02 µmol · g FW^{-1}) (Figure 2A). These values are consistent with experimental data for β-sitosterol (0.29 µmol · g FW^{-1}) but too low for campesterol and stigmasterol (experimental: 0.12 and 0.13 µmol · g FW^{-1}, respectively). The leaf model also predicted β-sitosterol to accumulate as the most prominent sterol (0.30 µmol · g FW^{-1}), campesterol at low levels (0.09 µmol · g FW^{-1}), and all other sterols at very low concentrations (< 0.05 µmol · g FW^{-1}) (Figure 2B). This was consistent with experimental data (β-sitosterol and campesterol at 0.30 and 0.07 µmol · g FW^{-1}, respectively). The predictions for stems were high β-sitosterol levels (0.65 µmol · g FW^{-1}) (very close to the measured concentration of 0.66 µmol · g FW^{-1}), relatively high campesterol quantities (0.19 µmol · g FW^{-1}) (close to the measured concentration of 0.15 µmol · g FW^{-1}), while other sterols were predicted to play less prominent roles (also in line with experimental data) (Figure 2C). Our model for sterol biosynthesis in seeds predicted high concentrations of β -sitosterol (5.8 µmol · g FW^{-1}) and considerable quantities of campesterol (1.3 µmol · g FW^{-1}) and stigmasterol (0.4 µmol · g FW^{-1}) as well, which matches experimental values for β -sitosterol and campesterol well (5.84 and 1.33 µmol · g FW^{-1}, respectively), but is too high for stigmasterol (experimental: 0.10 µmol · g FW^{-1}) (Figure 2D). Overall, the predicted sterol profiles were a fairly good match of the experimentally determined sterol accumulation patterns across organs. This is quite remarkable when considering that our simulations use numerous assumptions, the quality of which can be

219 substantially improved in future work. For example, the enzyme concentrations were estimated
220 based on previously published gene expression patterns (Schmid et al., 2005), and, while we
221 attempted to use similar growth conditions as reported in this publication, it is likely that the
222 crude gene-to-protein concentration conversion lacked accuracy. It is also conceivable that the
223 concentrations of sterol end products that directly affect biosynthetic enzymes by feedback
224 inhibition might be estimated incorrectly. Overall, we feel that our proof-of-concept models
225 certainly have utility for simulating sterol profiles and are an excellent first step toward truly
226 predictive kinetic models of sterol biosynthesis.
227
228 ***Ectopic* HMG1 *overexpression leads to increases in sterol levels but also to the accumulation of***
229 ***certain pathway intermediates***
230
231 Building on the initial successes with developing organ-specific models of sterol biosynthesis, we
232 attempted to predict the effects of gene overexpression on sterol profiles in transgenic
233 Arabidopsis plants. We recently reported on the generation and analysis of transgenics with
234 varying levels of expression of genes involved in isoprenoid precursor biosynthesis (Lange et al.,
235 2015) and selected the HMG1-6.1.7 line, which was shown to overexpress the *HMG1* gene in
236 rosette leaves, for further analysis (no other organs had been analyzed before). For the current
237 study, we employed quantitative real-time PCR to assess *HMG1* transcript levels. The *HMG1*
238 gene was found to be overexpressed in roots, rosette leaves, stems and seeds (25-, 26-, 49-, and
239 10-fold, respectively) (Figure 3A). Our prior work with kinetic models indicated that the
240 amplitude of transcript level variation appears to be larger than that of enzyme concentrations
241 in comparisons of wild-type versus transgenic plants (Rios-Estepa et al., 2008; Rios-Estepa et al,
242 2010). We therefore divided the fold-change for *HMG1* overexpression by a factor of 5 to
243 estimate the change in the concentration of the corresponding protein (5.0-, 5.2-, 9.8-, and 2.0-
244 fold for roots, leaves, stems and seeds, respectively). The only other adjusted model parameters
245 were kc40 (removes free sterols and decreasing feedback inhibition of biosynthetic enzymes by
246 accumulating end products) and the initial amount of acetyl-coenzyme A precursor available for
247 sterol pathway enzymes to act upon (reflects the experimentally determined increases of sterol
248 content in *HMG1* overexpressors over wild-type controls; 3.7-fold in roots, 3.0-fold in rosette
249 leaves, 3.3-fold in stems, and 1.6-fold in seeds) (Figure 3B). A detailed description of model
250 parameters is given in Supplemental Methods and Data File S1).
251
252 Root sterol concentrations for *HMG1* overexpressors were predicted to amount to 0.98 µmol
253 · g FW^{-1} for β-sitosterol and 0.18 µmol · g FW^{-1} for campesterol (Figure 4A), which were also the
254 principal sterols in experimental samples (0.99 and 0.40 µmol · g FW^{-1}, respectively). Our rosette
255 leaf model predicted an increase (when compared to wild-type controls) of β-sitosterol and
256 campesterol (0.65 and 0.18 µmol · g FW^{-1}, respectively) (Figure 4B), which was also close to
257 experimentally determined values (0.64 and 0.14 µmol · g FW^{-1}, respectively). When simulating
258 stem sterol profiles, β-sitosterol and campesterol concentrations were predicted to amount to
259 1.64 and 0.49 µmol · g FW^{-1}, respectively (Figure 4C), which closely matched experimental data
260 (1.64 and 0.40 µmol · g FW^{-1}, respectively). The model predictions for seeds were dramatically
261 increased concentrations of β-sitosterol and campesterol (8.2 and 1.8 µmol · g FW^{-1}, respectively)
262 (Figure 4D), again an excellent reflection of experimental measurements (8.31 and 1.88 µmol · g

FW^{-1}, respectively). Interestingly, all organ-specific models predicted a significant increase in the proportion of the sterol pathway intermediates, in particular cycloartenol, 24-methylene-cycloartanol and isofucosterol, in *HMG1* plants compared to wild-type controls. While these intermediates account for only a relatively small percentage of the total sterols in wild-type plants, we measured significant increases in *HMG1* plants, compared to controls, in all organs (cycloartenol, 6-11-fold; 24-methylenecycloartanol, 5-20-fold; isofucosterol, 2.6-180-fold) (Figure 5A-C). The accumulation of intermediates of sterol biosynthesis has been reported repeatedly for transgenic plants with increased flux into the pathway (by overexpression of one or more genes involved in precursor supply) (Chappell et al., 1995; Holmberg et al., 2003; Lange et al., 2015). When a gene that encodes a protein that turns over an accumulated intermediate (such as SMO1 for cycloartenol and 24-methylenecycloartanol, SMT1 for cycloartenol, or DWF1 for isofucosterol) was overexpressed in plants already overexpressing *HMG1*, flux constraints could be partially removed and additional increases in sterol end products were observed (Holmberg et al., 2003; Lange et al., 2015). In summary, our models have been remarkably accurate with predicting sterol profiles across organs and genotypes. If more accurate data sets of enzyme concentrations were to be integrated into these models, the predictive power would likely increase as well. In our opinion, the fact that the accumulation of sterol pathway intermediates was correctly predicted indicates that kinetic modeling can point to potential flux bottlenecks, thereby suggesting experimental approaches toward flux enhancement. It will now be interesting to evaluate if a combination of modeling and experimentation has the potential to speed up metabolic engineering by being able to focus on the most promising avenues for the accumulation of desirable metabolites.

Materials and Methods

Plant growth for harvest of aboveground tissue samples

Seeds of wild-type and homozygous transgenic lines were germinated in soil (6 x 6 cm pots) and maintained in a growth chamber (16 h day/8 h night photoperiod; 100 µmol m^{-2} s^{-1} light intensity at soil level; constant temperature at 23°C; 70% relative humidity). Pots were arranged in a random grid and rotated once a day. Rosette leaves were collected at growth stage 5.10 (just as the inflorescence starts to appear; Boyes et al., 2001); stems and siliques were collected at growth stage 6.50 from a separate set of plants. Developing seeds were separated from siliques using a rapid separation procedure (Bates et al., 2013). Mature seeds were collected at growth stage 9.70 from yet another set of plants. Leaf and stem tissue samples were used for both qPCR and metabolite analyses. Immature seeds were used for qPCR expression analysis (during seed filling), whereas mature seeds were used for metabolite analyses. Samples were shock-frozen in liquid nitrogen immediately following harvest, the frozen tissue samples homogenized with mortar and pestle in the presence of liquid nitrogen, and aliquots of the resulting homogenate stored in 2 ml Eppendorf tubes at -80°C. Samples were further homogenized (Ball Mill MM301, Retsch) before subsequent analyses. Samples were harvested from three independent experiments (biological replicates).

Plant growth for harvest of root tissue

Plants were grown in an aeroponic culture system (according to Vaughan et al., 2011) using the same lighting conditions as described above. Briefly, plants were grown in soil for 3 weeks, then removed from soil and transplanted into 50 ml conical vials containing Seramis clay granulate, with holes punched into the bottom for water access. The vials were placed in a solution of half-strength MS basal salt for 10 min once every 48 h. Pots and vials were arranged in a random grid and rotated once a day. After 3 weeks of growth in the aeroponic system, plants were removed from the vials and roots were separated from the Seramis granules for harvest. Root tissue was harvested, homogenized and stored as described above.

Quantitative real-time PCR

Root, rosette and stem RNA was extracted using the Trizol reagent (Life Technologies) according to the manufacturer's instructions. RNA extraction from seeds involved a two-step Trizol-based procedure (Meng and Feldmann, 2010). Isolated RNA (1,000 ng) was treated with RNase-free DNase (Thermo Scientific) and first strand cDNA synthesized using Superscript III reverse transcriptase (Life Technologies). In a 10-µL quantitative PCR reaction, concentrations were adjusted to 150 nM (primers), 1 x Power SYBR Green PCR Master Mix (Life Technologies), and 10 x diluted first strand cDNA as template (primer sequences provided in Table S1). Reactions were performed in a 96-well optical plate at 95°C for 10 min, followed by 40 cycles of 95°C for 15 s and 60°C for 10 min in a 7500 Real-Time PCR system (Life Technologies). Fluorescence intensities of three independent measurements (technical replicates) were normalized against the ROX reference dye (ThermoFisher Scientific). Relative transcript levels were calculated based on the comparative CT method as specified in the manufacturer's instructions (Life Technologies). β-Actin (At3g18780) served as the constitutively expressed endogenous control and the expression level of the corresponding wild-type allele was used as the calibrator in these calculations.

Sterol analyses

Tissue homogenate (60–70 mg for root, leaf and stem; 10 mg for seed) was extracted at 75°C for 60 min with 4ml of $CHCl_3$/MeOH (2:1, v:v; containing 1.25 mg · L^{-1} epi-cholesterol as internal standard). Samples were evaporated to dryness (EZ2-Bio, GeneVac), and the remaining residue was saponified at 90°C for 60 min in 2 ml of 6% (w/v) KOH in MeOH. Upon cooling to room temperature, 1 ml of hexane and 1 ml of H_2O were added, and the mixture was shaken vigorously for 20 s. Following centrifugation (3,000 x *g* for 2 min) for phase separation, the hexane phase was transferred to a 2 ml glass vial, and the aqueous phase re-extracted with 1 ml of hexane as above. The mixture was centrifuged as above, the hexane phase removed and added to the 2 ml glass vial containing the hexane phase from the first extraction. The combined organic phases were evaporated to dryness as above, 50 µl of N-Methyl-N-(trimethylsilyl)trifluoroacetamide were added to the residue, the mixture was shaken vigorously for 20 s, and the sample then transferred to a 2 ml glass vial with a 100-µl conical glass insert. After capping the vial, the reaction mixture was incubated at room temperature for 5 min. Gas chromatography-mass spectrometry analyses were performed on an Agilent 6890N gas chromatograph coupled to an

Agilent 5973 inert mass selective detector (MSD) detector. Samples were loaded (injection volume 1 µl) with a LEAP CombiPAL autosampler onto an Agilent HP-5MS fused silica column (30 m x 250 mm; 0.25-mm film thickness). The temperatures of the injector and MSD interface were both set to 280°C. Analytes were separated at a flow rate of 1 ml · min^{-1}, with He as the carrier gas, using a thermal gradient starting at 170°C (hold for 1.5 min), a first ramp from 170°C to 280°C at 37°C/min, a second ramp from 280°C to 300°C at 1.5°C/min, and a final hold at 300°C for 5.0 min. Eluting metabolites were fragmented in electron impact mode with an ionization voltage of 70 eV and data was acquired using MSD ChemStation software (revision D.01.02.SP1, Agilent Technologies). Analytes were identified based on their mass fragmentation patterns by comparison with those of authentic standards using the National Institute of Standards and Technology Mass Spectral Search Program (version D.05.00). Peak areas were obtained from the total ion chromatogram for all detectable peaks with a sterol mass fragmentation signature. Raw data were exported to Microsoft Excel and peak areas normalized to tissue mass and internal standard. A blank injection was performed after each sample run, and the background signal from the blank subtracted from the sample values for the entire run. Prior to sample analyses, and then after every 20 samples, a standard mix was run to evaluate the reproducibility of the analyses. Absolute quantitation of sterols was achieved based on calibration curves obtained with authentic standards.

Development of organ-specific kinetic models of sterol biosynthesis

Publicly available information regarding the biochemical properties of enzymes involved in sterol biosynthesis (Michaelis constant, turnover number, and inhibition constant) was assembled from the literature and the BRENDA repository (https://www.brenda-enzymes.org/). The information was then further consolidated by prioritizing kinetic values from Arabidopsis, Brassicaceae, plants and other eukaryotes (in this order). For each reaction of the sterol pathway, the concentration change of reactants over time was defined according to the Michaelis-Menten formalism, as developed by Briggs and Haldane (Fersht, 1985), and converted into ODEs. These were then integrated into a system of interdependent ODEs and numerical solutions obtained in MATLAB version 7.12.0.635 (MathWorks) using the ode15s solver. The full MATLAB code, with explanations, is provided in Supplemental Methods and Data File S1. Simulations were performed assuming a 50 d (7 week) growth period. The following files, functions, parameters and variables were generated within MATLAB:

Script File. A set of commands that includes the vector for pathway metabolites, time span, and the vector of initial conditions. It calls the function (m-file) that solves the ODEs and produces the graphical outputs (monoterpene profiles).

Function (m-file). Inputs: independent variable ***t*** (time span); vector of dependent variables ***x*** ([Metabolites]). Solves the set of ODEs with the initial values given in the vector of initial conditions. Returns the values of the independent variable in the vector ***t*** (time span) and the values of the dependent variables in the vector ***x*** ([Metabolites]). The vector of independent variables ***t*** is not equally spaced because the function (m-file) controls the step size.

Fixed parameters. Kinetic constants of enzymes involved in sterol biosynthesis.

Non-constant parameters (variables). Enzyme concentrations for each organ and genotype. Factor kc40 to account for the conversion of frees sterols into sterol esters and incorporation into membranes, thereby reducing the concentration of sterol pathway end products that can act on biosynthetic enzymes via feedback inhibition. Initial amount of starting material (acetyl-CoA) in the script file (all other metabolite concentrations are set to 0 at t_0).

Acknowledgements

This work was supported by the National Science Foundation (grant no. NSF-MCB-090758 to B.M.L.).

Author Contributions

BML conceived of the project. BCP and IL designed and performed the experimental work. RRE and RS developed the kinetic mathematical models. All authors were involved in data analysis. BML wrote the manuscript, with contributions from all other authors.

Table 1. Sterol and triterpenoid levels in different Arabidopsis organs (n = 6-10; values indicate averages and standard errors).

Organ	Total sterols [µmol g FW^{-1}]	Sterol composition [% of total]									
		Pathway end products					Pathway intermediates		Triterpenoids		Other
		Sitosterol	Campesterol	Cholesterol	Stigmasterol	Brassicasterol	Cycloartenol	Isofucosterol	β-Amyrin	Lupeol	
Roots	0.6 ± 0.1	48.3 ± 4.5	19.4 ± 1.6	1.3 ± 0.3	22.0 ± 2.0	< 0.1	5.0 ± 1.2	< 0.1	2.2 ± 0.8	0.4 ± 0.4	1.4
Leaves	0.4 ± 0.1	70.3 ± 16.8	16.4 ± 4.8	2.3 ± 0.9	< 0.1	< 0.1	4.4 ± 1.8	5.1 ± 2.9	< 0.1	1.5 ± 0.7	< 0.1
Stems	1.0 ± 0.1	63.5 ± 7.7	14.0 ± 1.5	2.0 ± 0.2	< 0.1	8.8 ± 1.0	6.2 ± 0.9	< 0.1	5.0 ± 0.6	< 0.1	0.5
Seed	8.2 ± 1.0	69.8 ± 3.6	15.8 ± 3.3	3.3 ± 1.8	1.2 ± 0.4	1.0 ± 0.2	2.5 ± 0.9	3.7 ± 3.6	1.8 ± 1.4	0.2 ± 0.2	0.7

Table 2. Kinetic properties of sterol pathway enzymes (values with asterisks have been determined experimentally, all others are estimated). The units are uM (K_M), nmol min^{-1} mg protein^{-1} (V_{max}), and s-1 (k_{cat}). The numbering of enzymes is in accordance with the scheme shown in Figure 1. Abbreviations: DMAPP, dimethylallyl diphosphate; FPP, farnesyl diphosphate; GPP, geranyl diphosphate; HMG-CoA, 3-hydroxy-3-methylglutaryl-coenzyme A; IPP, isopentenyl diphosphate; MP, microsomal preparation; MVA, mevalonate; PNE, purified native enzyme; PRE, purified recombinant enzyme.

#	Enzyme	K_M	V_{max}	k_{cat}	Comments	References
1	Acetoacetyl-CoA thiolase (AACT)	770* (Candida tropicalis; PNE)	-	2.1*		Kanayama et al. (1997)
2	3-Hydroxy-3-methylglutaryl-CoA synthase (HMGS)	43* (Brassica juncea; PNE)	470*	0.415*	competitive inhibition by HMG-CoA (Ki = 9)	Nagegowda et al. (2004)
3	3-Hydroxy-3-methylglutaryl-CoA reductase (HMGR)	27* (Raphanus sativus; PNE)	11*	0.02	competitive inhibition by MVA (Ki = 990)	Bach et al. (1986)
4	Mevalonate kinase (MK)	76* (Catharanthus roseus; PNE)	13.6*	0.02	competitive inhibition by FPP (Ki = 0.1)	Schulte et al. (2000)
5	Phosphomevalonate kinase (PMK)	42* (Hevea brasiliensis; PNE)	2.6*	0.02		Skilleter et al. (1971)
6	Mevalonate diphosphate decarboxylase (MPDC)	10* (Cymbopogon citratus; PNE)	1.12*	0.02		Lalitha et al. (1985)
7	Isopentenyl diphosphate: dimethylallyl diphosphate isomerase (IPPI)	5.1* IPP, 17.0* DMAPP (Cinchona robusta; PNE)	19.8*	0.89*	uni-uni mechanism	Ramos-Valvidia et al. (1997)
8	Farnesyl diphosphate synthase (FPPS)	15.3* IPP, 9.0* DMAPP, 1.8* GPP (Abies grandis; PNE)	0.84*	1.0* IPP, 9.0* DMAPP		Tholl et al. (2001)
9	Squalene synthase (SQS)	9.5* FPP (Nicotiana tabacum; PNE)	-	0.53*		Hanley and Chappell (1992)
10	Squalene monooxygenase / squalene epoxidase (SQE)	7.7* (Homo sapiens; PRE)	-	0.0183*		Laden et al. (2000)
11	Cycloartenol synthase (CAS)	125* (Zea mays; PNE)	-	0.015		Abe et al. (1988)
12	Cycloartenol C24 methyltransferase (SMT1)	30* (Zea mays; PNE)	0.02*	0.01*	competitive inhibition by 24-methylenecylcoartenol (Ki = competitive inhibition by 24-ethylidenelophenol (Ki = 50) competitive inhibition by sitosterol (Ki = 100)	Nes et al. (2003); Zhou and Nes (2003); Neelandankan et al. (2009); Parker and Nes (1992)
13	Sterol 4α demethylase complex (SMO1)	500* (Zea mays; MP)	0.135*	0.06	competitive inhibition by sitosterol (Ki = 100)	Pascal et al. (1993); Rahier et al. (2006); d'Andréa et al. (2007)
14	Cycloeucalenol cycloisomerase (CECI)	100* (Zea mays; MP)	0.6*	0.05		Rahier et al. (1989)
15	Obtusifoliol C14 demethylase (CYP51)	160* (Zea mays; MP)	0.065*	0.05		Taton and Rahier (1991)
16	Sterol C14 reductase (FACKEL)	100* (Zea mays; MP)	0.23*	0.05		Taton et al. (1989)
17	C-8,7 Sterol isomerase (HYDRA)	75* (Zea mays; MP)	0.2*	0.05		Rahier et al. (1997)
18	Sterol C24-methyltransferase (SMT2)	28* methylene lophenol (Arabidopsis thaliana; PRE)	-	0.01*	competitive inhibition by sitosterol (Ki = 300)	Zhou and Nes (2003); Parker and Nes
19	Δ7-Sterol C5-desaturase (DWF7) (campesterol	115* Cholesten-7-en-3beta-ol (Zea mays; MP)	0.13	0.06		Taton and Rahier (1996)
20	Sterol Δ7-reductase (DWF5) (campesterol branch)	460* (Zea mays; MP)	0.61	0.06		Taton and Rahier (1991)
21	Sterol C24-reductase (DWF1) (campesterol branch)	150	-	0.06		-
22	Conversion of campersterol into brassinosteroids	(considered as not carrying significant flux)	-	-		-
23	Sterol 4α demethylase complex (SMO2)	480* (Zea mays; MP)	0.16	0.06		Pascal et al. (1993); Pascal et al. (1994)
24	Δ^7-Sterol C5-desaturase (DWF7) (sitosterol branch)	140* Stigmasta-7,24(24')-dien-3beta-ol (Zea mays;	0.13	0.06		Taton and Rahier (1996)
25	Sterol Δ^7-reductase (DWF5) (sitosterol branch)	460* (Zea mays; MP)	0.61	0.06		Taton and Rahier (1991)
26	Sterol C24-reductase (DWF1) (sitosterol branch)	150	-	0.0018		-
27	Sterol C22-desaturase (CYP710A)	1.0* (Arabidopsis thaliana; PRE)	-	0.0001		Morikawa et al. (2006)
28	Sterol C24-methyltransferase (SMT2)	28 episterol (Arabidopsis thaliana; PRE)	-	0.01*		Nes et al. (2003)
29	Sterol C24-methyltransferase (SMT2)	28 5-dehydroepisterol (Arabidopsis thaliana; PRE)	-	0.01*		Nes et al. (2003)
30	Sterol C24-methyltransferase (SMT2)	28 24-methylene cholesterol (Arabidopsis thaliana;	-	0.01*		Nes et al. (2003)

Table 3. Expression levels of sterol biosynthetic genes in different organs and conversion into enzyme concentrations (for legend of abbreviations see Table 2). The numbering of genes is in accordance with that of the corresponding enzymes in Figure 1.

#	AGI	Annotation	Annotation quality	Transcript level (roots)	Enzyme conc. [µM]	Transcript level (rosette leaves)	Enzyme conc. [µM]	Transcript level (stems)	Enzyme conc. [µM]	Transcript level (seeds)	Enzyme conc. [µM]
1	At5g47720	AACT	by homology	689.01	0.1013	121.30	0.0178	550.59	0.0810	487.88	0.0717
1	At5g48230	AACT	by homology	1008.60	0.1483	275.24	0.0405	298.70	0.0439	374.32	0.0550
				Sum (active)	0.2496	Sum (active)	0.0583	Sum (active)	0.1249	Sum (active)	0.1268
2	At4g11820	HMGS	functional	1223.12	0.1799	464.49	0.0683	565.22	0.0831	1126.38	0.1656
3	At1g76490	HMGR	functional	2156.62	0.3171	1532.79	0.2254	1547.13	0.2275	854.06	0.1256
3	At2g17370	HMGR	functional	214.44	0.0315	66.44	0.0098	80.01	0.0118	221.27	0.0325
				Sum (active)	0.3487	Sum (active)	0.2352	Sum (active)	0.2393	Sum (active)	0.1581
4	At5g27450	MK	functional	603.91	0.0888	180.28	0.0265	180.27	0.0265	192.18	0.0283
5	At1g31910	PMK	by homology	2326.96	0.3422	1720.70	0.2530	2046.61	0.3010	1319.80	0.1941
6	At2g38700	MPDC	functional	982.95	0.1446	255.87	0.0376	313.04	0.0460	220.53	0.0324
6	At3g54250	MPDC	by homology	131.23	0.0193	56.26	0.0083	108.79	0.0160	66.31	0.0098
				Sum (active)	0.1638	Sum (active)	0.0459	Sum (active)	0.0620	Sum (active)	0.0422
7	At3g02780	IPPI	functional	2332.69	0.3430	767.77	0.1129	633.93	0.0932	817.99	0.1203
7	At5g16440	IPPI	functional	386.54	0.0568	256.75	0.0378	274.59	0.0404	183.37	0.0270
				Sum (active)	0.3999	Sum (active)	0.1507	Sum (active)	0.1336	Sum (active)	0.1473
8	At4g17190	FPPS	functional	443.96	0.0653	301.11	0.0443	304.47	0.0448	158.65	0.0233
8	At5g47770	FPPS	functional	1658.74	0.2439	719.90	0.1059	823.80	0.1211	89.63	0.0132
				Sum (active)	0.3092	Sum (active)	0.1501	Sum (active)	0.1659	Sum (active)	0.0365
9	At4g34640	SQS	functional	896.50	0.1318	411.44	0.0605	461.85	0.0679	194.41	0.0286
	At4g34650		pseudogene	not considered	-	-	-	-	-	-	-
#	At1g58440	SQE	functional	470.81	0.0692	289.60	0.0426	257.90	0.0379	313.76	0.0461
#	At2g22830	SQE	functional	39.91	0.0059	60.55	0.0089	42.46	0.0062	30.23	0.0044
#	At4g37760	SQE	functional	124.69	0.0183	599.12	0.0881	436.14	0.0641	817.30	0.1202
	At5g24140	SQE	no SQE act.	44.77	0.0066	3.58	0.0005	3.41	0.0005	3.55	0.0005
	At5g24150	SQE	no SQE act.	17.16	0.0025	953.12	0.1402	551.95	0.0812	96.00	0.0141
	At5g24160	SQE	no SQE act.	34.71	0.0051	142.12	0.0209	68.92	0.0101	33.32	0.0049
				Sum (active)	0.0934	Sum (active)	0.1396	Sum (active)	0.1083	Sum (active)	0.1708
#	At2g07050	CAS	functional	1012.28	0.1489	944.59	0.1389	1027.42	0.1511	775.61	0.1141
#	At5g13710	SMT1	functional	1694.35	0.2492	1202.51	0.1768	1375.55	0.2023	443.39	0.0652
#	At4g12110	SMO1	functional	388.97	0.0572	377.76	0.0556	609.03	0.0896	196.82	0.0289
#	At4g22753	SMO1	by homology	8.34	0.0012	200.06	0.0294	117.44	0.0173	138.24	0.0203
#	At4g22756	SMO1	functional	224.12	0.0330	177.48	0.0261	231.33	0.0340	173.19	0.0255
				Sum (active)	0.0914	Sum (active)	0.1111	Sum (active)	0.1409	Sum (active)	0.0747
#	At5g50375	CECI	functional	340.52	0.0501	142.77	0.0210	198.75	0.0292	89.22	0.0131
#	At1g11680	CYP51	functional	1266.59	0.1863	673.15	0.0990	858.30	0.1262	862.64	0.1269
#	At3g52940	FACKEL	functional	354.05	0.0521	309.36	0.0455	226.15	0.0333	132.83	0.0195
	At2g17330		pseudogene	not considered	-	-	-	-	-	-	-
#	At1g20050	HYDRA	functional	1885.62	0.2773	901.19	0.1325	1035.43	0.1523	526.94	0.0775
#	At1g20330	SMT2	functional	1232.41	0.1812	1412.29	0.2077	989.16	0.1455	904.88	0.1331
#	At1g76090	SMT3	functional	1531.85	0.2253	409.57	0.0602	710.91	0.1045	1305.52	0.1920
				Sum (active)	0.4065	Sum (active)	0.2679	Sum (active)	0.2500	Sum (active)	0.3251
19	At3g02580	DWF7	functional	722.53	0.1063	362.27	0.0533	367.30	0.0540	589.97	0.0868
19	At3g02590	DWF7	by homology	9.60	0.0014	8.46	0.0012	8.12	0.0012	30.70	0.0045
				Sum (active)	0.1077	Sum (active)	0.0545	Sum (active)	0.0552	Sum (active)	0.0913
20	At1g50430	DWF5	functional	1312.59	0.1930	1098.55	0.1616	908.51	0.1336	579.39	0.0852
21	At3g19820	DWF1	functional	4359.74	0.6411	1854.24	0.2727	1934.37	0.2845	1186.09	0.1744
#	Conversion of campesterol to brassinolides is not considered as carrying significant flux.										
#	At1g07420	SMO2	functional	349.37	0.0514	202.89	0.0298	248.08	0.0365	488.42	0.0718
#	At2g29390	SMO2	functional	421.96	0.0621	272.85	0.0401	267.05	0.0393	319.66	0.0470
				Sum (active)	0.1134	Sum (active)	0.0700	Sum (active)	0.0758	Sum (active)	0.1188
#	At2g34500	CYP710	functional	250.94	0.0369	5.15	0.0008	9.06	0.0013	5.74	0.0008
#	At2g34490	CYP710	functional	317.61	0.0467	65.79	0.0097	329.61	0.0485	194.35	0.0286
#	At2g28860	CYP710	functional	12.98	0.0019	8.90	0.0013	7.99	0.0012	8.79	0.0013
				Sum (active)	0.0855	Sum (active)	0.0117	Sum (active)	0.0510	Sum (active)	0.0307

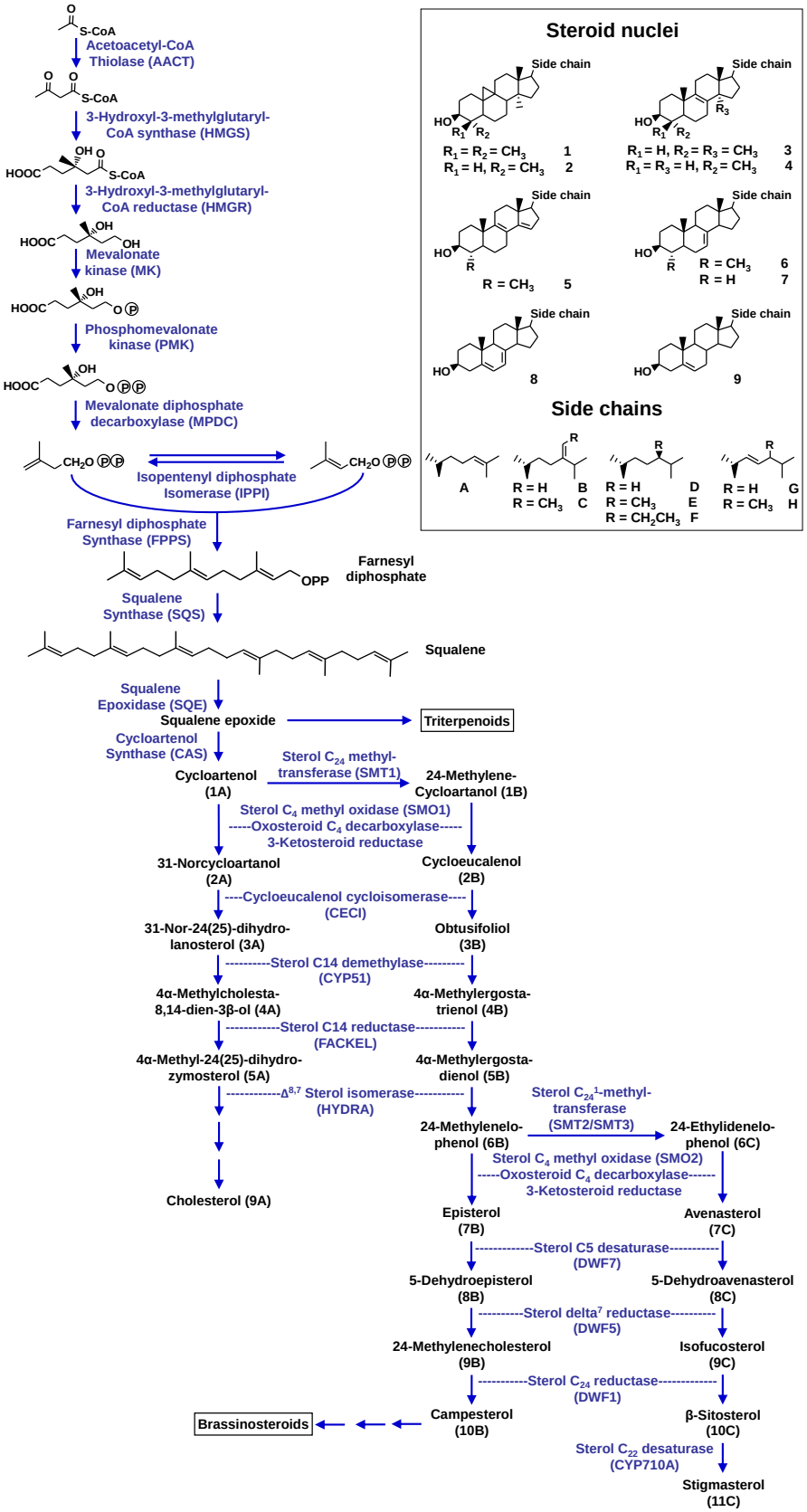

Figure 1. Outline of the core sterol biosynthetic pathway in plants.

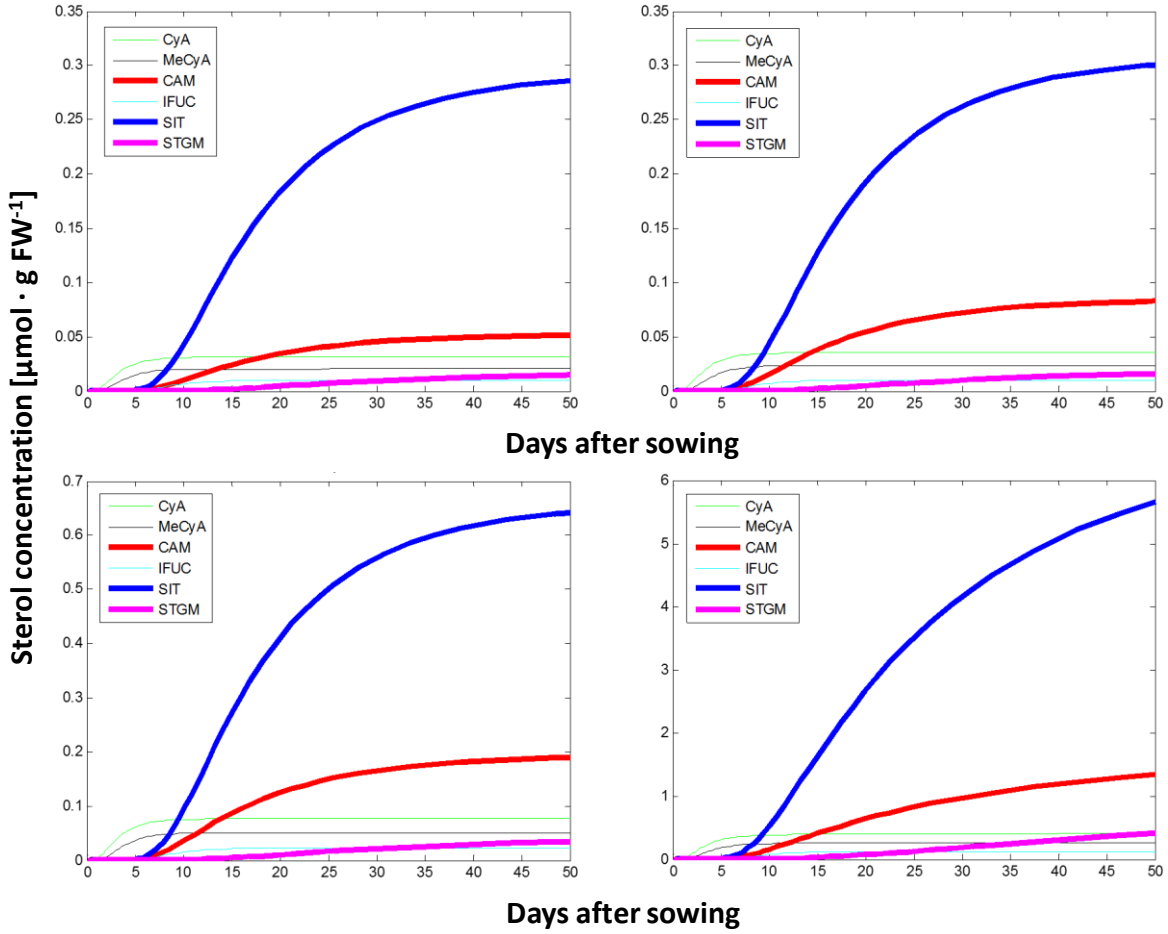

Figure 2. Prediction of sterol profiles, using kinetic mathematical modeling, in different organs of Arabidopsis. **A**, roots; **B**, rosette leaves; **C**, stems; and **D**, seeds. Abbreviations: CAM, campesterol; CyA, cycloartenol; IFUC, isofucosterol; MeCyA, 24-methylenecycloartanol; SIT, β-sitosterol; STGM, stigmasterol.

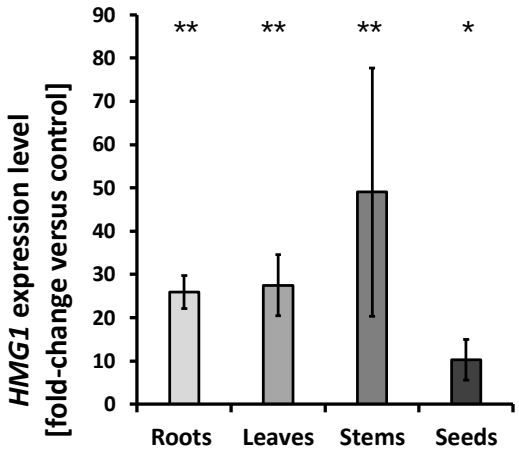

Figure 3. Analysis of Arabidopsis organ samples of wild-type controls and plants overexpressing the *HMG1* gene. **A**, Expression patterns of the *HMG1* gene (n = 3) and **B**, sterol content (n = 10) (both expressed as fold-change overexpressor versus control). Standard errors shown as bars; asterisks indicate the level of significance in a Student's t test (*, $P \leq 0.01$; and **, $P \leq 0.001$).

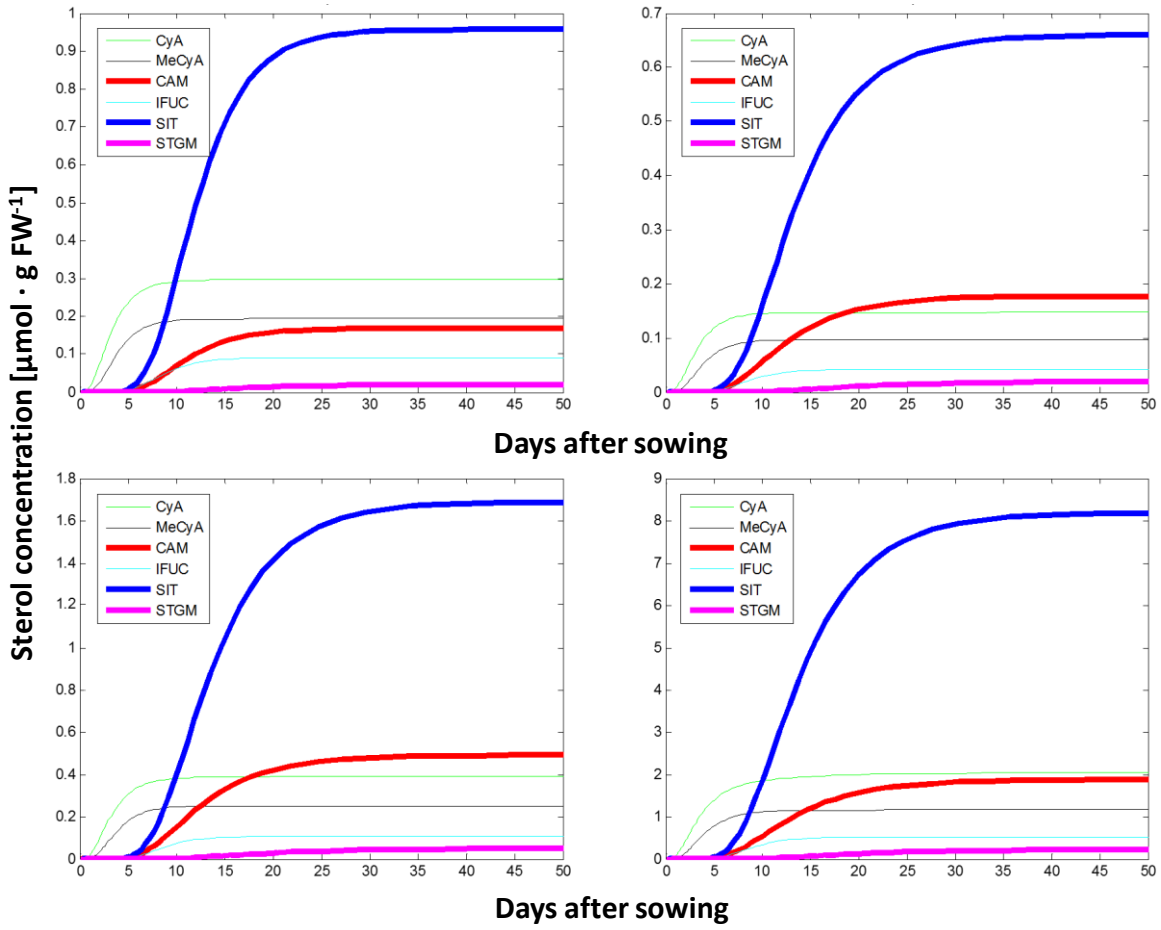

Figure 4. Prediction of sterol profiles, using kinetic mathematical modeling, in different organs of transgenic Arabidopsis plants overexpressing the *HMG1* gene. **A**, roots; **B**, rosette leaves; **C**, stems; and **D**, seeds. Abbreviations: CAM, campesterol; CyA, cycloartenol; IFUC, isofucosterol; MeCyA, 24-methylenecycloartanol; SIT, β-sitosterol; STGM, stigmasterol.

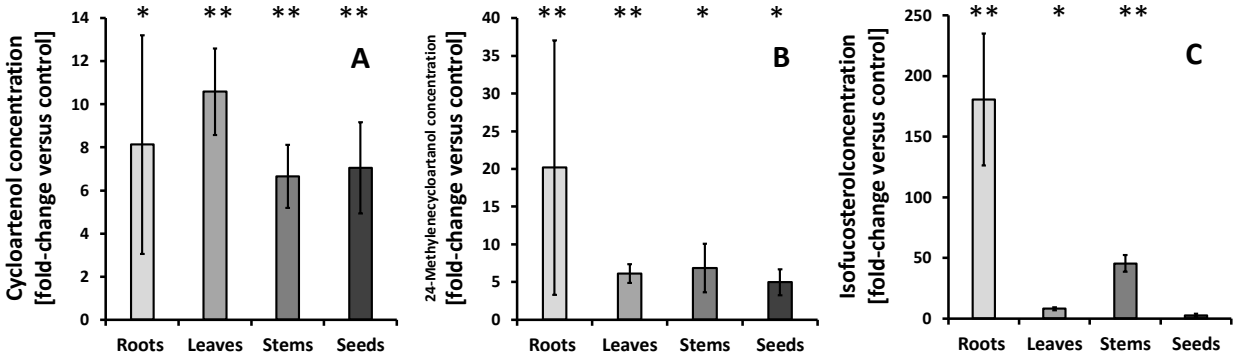

Figure 5. Analysis of sterol pathway intermediates of wild-type controls and plants overexpressing the *HMG1* gene. **A**, cycloartenol; **B**, 24-methylenecycloartanol; **C**, isofucosterol (all expressed as fold-change overexpressor versus control; n = 10). Standard errors shown as bars; asterisks indicate the level of significance in a Student's t test (*, $P \leq 0.01$; and **, $P \leq 0.001$; n = 6-10).

REFERENCES

Arnqvist L, Persson M, Jonsson L, Dutta PC, Sitbon F (2008) Overexpression of CYP710A1 and CYP710A4 in transgenic *Arabidopsis* plants increases the level of stigmasterol at the expense of sitosterol. Planta 227: 309-317

Babiychuk E, Bouvier-Navé P, Compagnon V, Suzuki M, Muranaka T, Van Montagu M, Kushnir S, Schaller H (2008) Allelic mutant series reveal distinct functions for *Arabidopsis* cycloartenol synthase 1 in cell viability and plastid biogenesis. Proc Natl Acad Sci USA 105: 3163-3168

Bates PD, Jewell JB and Browse J (2013) Rapid separation of developing Arabidopsis seeds from siliques for RNA or metabolite analysis. Plant Methods 9: 9

Bessueille L, Sindt N, Guichardant M, Djerbi S, Teeri TT, Bulone V (2009) Plasma membrane microdomains from hybrid aspen cells are involved in cell wall polysaccharide biosynthesis. Biochem J 420: 93-103

Bouvier-Navé P, Husselstein T, Desprez T, Benveniste P (1997) Identification of cDNAs encoding sterol methyl-transferases involved in the second methylation step of plant sterol biosynthesis. Eur J Biochem 246: 518-529

Boyes DC, Zayed AM, Ascenzi R, McCaskill AJ, Hoffman NE, Davis KR, Görlach J (2001) Growth stage-based phenotypic analysis of Arabidopsis: a model for high throughput functional genomics in plants. Plant Cell 13: 1499-1510

Busquets A, Keim V, Closa M, Del Arco A, Boronat A, Arró M, Ferrer A (2008) *Arabidopsis thaliana* contains a single gene encoding squalene synthase. Plant Mol Biol 67: 25-36.

Chappell J, Wolf F, Proulx J, Cuellar R, Saunders C (1995) Is the reaction catalyzed by 3-hydroxy-3-methylglutaryl coenzyme A reductase a rate-limiting step for isoprenoid biosynthesis in plants? Plant Physiol 109: 1337-1343

Chen Q, Steinhauer L, Hammerlindl J, Keller W, Zou J (2007) Biosynthesis of phytosterol esters: identification of a sterol o-acyltransferase in Arabidopsis. Plant Physiol 145: 974-984

Choe S, Noguchi T, Fujioka S, Takatsuto S, Tissier CP, Gregory BD, Ross AS, Tanaka A, Yoshida S, Tax FE, Feldmann KA (1999a) The *Arabidopsis* dwf7/ste1 mutant is defective in the delta7 sterol C-5 desaturation step leading to brassinosteroid biosynthesis. Plant Cell 11: 207-221

Choe S, Dilkes BP, Gregory BD, Ross AS, Yuan H, Noguchi T, Fujioka S, Takatsuto S, Tanaka A, Yoshida S, et al (1999b) The Arabidopsis dwarf1 mutant is defective in the conversion of 24-methylenecholesterol to campesterol in brassinosteroid biosynthesis. Plant Physiol 119: 897–907

Choe S, Tanaka A, Noguchi T, Fujioka S, Takatsuto S, Ross AS, Tax FE, Yoshida S, Feldmann KA (2000) Lesions in the sterol delta reductase gene of *Arabidopsis* cause dwarfism due to a block in brassinosteroid biosynthesis. Plant J 21: 431-443

d'Andréa S, Canonge M, Beopoulos A, Jolivet P, Hartmann MA, Miquel M, Lepiniec L, Chardot T (2007) At5g50600 encodes a member of the short-chain dehydrogenase reductase superfamily with 11beta- and 17beta-hydroxysteroid dehydrogenase activities associated with Arabidopsis thaliana seed oil bodies. Biochimie 89: 222-229

453 Darnet S, Bard M, Rahier A (2001) Functional identification of sterol-4alpha-methyl oxidase
454 cDNAs from *Arabidopsis thaliana* by complementation of a yeast erg25 mutant lacking sterol-
455 4alpha-methyl oxidation. FEBS Lett 508: 39-43
456 Darnet S, Rahier A (2004) Plant sterol biosynthesis: identification of two distinct families of sterol
457 4alpha-methyl oxidases. Biochem J 378: 889-898
458 Diener AC, Li H, Zhou W, Whoriskey WJ, Nes WD, Fink GR (2000) Sterol methyltransferase 1
459 controls the level of cholesterol in plants. Plant Cell 12: 853-870
460 Fersht A (1985) Enzyme structure and mechanism, W.H. Freeman, New York, 475 pages
461 Gachotte D, Meens R, Benveniste P (1995) An Arabidopsis mutant deficient in sterol biosynthesis:
462 heterologous complementation by ERG 3 encoding a delta7-sterol-C-5-desaturase from
463 yeast. Plant J 8: 407-416
464 Gachotte D, Husselstein T, Bard M, Lacroute F, Benveniste P (1996) Isolation and characterization
465 of an *Arabidopsis thaliana* cDNA encoding a delta 7-sterol-C-5-desaturase by functional
466 complementation of a defective yeast mutant. Plant J 9: 391-398
467 Georg HB, Sherrier DJ, Weimar T, Louise VM, Hawkins ND, MacAskill A, Napier JA, Beale MH, Lilley
468 KS, Dupree P (2005) Analysis of detergent-resistant membranes in Arabidopsis; evidence for
469 plasma membrane lipid rafts. Plant Physiol 137: 104-116
470 Grebenok RJ, Ohnmeiss TE, Yamamoto A, Huntley ED, Galbraith DW, DellaPenna D (2000)
471 Isolation and characterization of an *Arabidopsis thaliana* C-8,7 sterol isomerase: functional
472 and structural similarities to mammalian C-8,7 sterol isomerase /emopamil-binding protein.
473 Plant Mol Biol 38: 807-815
474 Hemmerlin A, Harwood JL, Bach TJ (2012) A raison d'être for two distinct pathways in the early
475 steps of plant isoprenoid biosynthesis? Prog Lipid Res 51: 95-148
476 Hey SJ, Powers SJ, Beale MH, Hawkins ND, Ward JL, Halford NG (2006) Enhanced seed sterol
477 accumulation through expression of a modified HMG-CoA reductase. Plant Biotechnol J 4:
478 219-229
479 Holmberg N, Harker M, Wallace AD, Clayton JC, Gibbard CL, Safford R (2003) Co-expression of N-
480 terminal truncated 3-hydroxy-3-methylglutaryl CoA reductase and C24-sterol
481 methyltransferase type 1 in transgenic tobacco enhances carbon flux towards end-product
482 sterols. Plant J 36: 12-20
483 Husselstein T, Gachotte D, Desprez T, Bard M, Benveniste P (1996) Transformation of
484 *Saccharomyces cerevisiae* with a cDNA encoding a sterol C-methyltransferase from
485 Arabidopsis thaliana results in the synthesis of 24-ethyl sterols. FEBS Lett 381: 87-92
486 Husselstein T, Schaller H, Gachotte D, Benveniste P (1999) Delta7-sterol-C5-desaturase:
487 molecular characterization and functional expression of wild-type and mutant alleles. Plant
488 Mol Biol 39: 891-906
489 Jang JC, Fujioka S, Tasaka M, Seto H, Takatsuto S, Ishii A, Aida M, Yoshida S, Sheen J (2000) A
490 critical role of sterols in embryonic patterning and meristem programming revealed by the
491 fackel mutants of Arabidopsis thaliana. Genes Dev 14: 1485-1497
492 Jiang W and Lin W (2013) Brassinosteroid functions in Arabidopsis seed development. Plant Signal
493 Behav 8: 10
494 Kierszniowska S, Seiwert B, Schulze WX (2009) Definition of Arabidopsis sterol-rich membrane
495 microdomains by differential treatment with methyl-beta-cyclodextrin and quantitative
496 proteomics. Mol Cell Proteomics 8: 612-623

Kim HB, Schaller H, Goh CH, Kwon M, Choe S, An CS, Durst F, Feldmann KA, Feyereisen R (2005) *Arabidopsis* cyp51 mutant shows postembryonic seedling lethality associated with lack of membrane integrity. Plant Physiol 138: 2033-2047

Klahre U, Noguchi T, Fujioka S, Takatsuto S, Yokota T, Nomura T, Yoshida S, Chua NH (1998) The *Arabidopsis* DIMINUTO/DWARF1 gene encodes a protein involved in steroid synthesis. Plant Cell 10: 1677-1690

Kribii R, Arró M, Del Arco A, González V, Balcells L, Delourme D, Ferrer A, Karst F, Boronat A (1997) Cloning and characterization of the *Arabidopsis thaliana* SQS1 gene encoding squalene synthase - involvement of the C-terminal region of the enzyme in the channeling of squalene through the sterol pathway. Eur J Biochem 249: 61-69

Kushiro M, Nakano T, Sato K, Yamagishi K, Asami T, Nakano A, Takatsuto S, Fujioka S, Ebizuka Y, Yoshida S (2001) Obtusifoliol 14alpha-demethylase (CYP51) antisense *Arabidopsis* shows slow growth and long life. Biochem Biophys Res Commun 285: 98-104

Lange BM, Rios-Estepa R (2014) Kinetic modeling of plant metabolism and its predictive power: peppermint essential oil biosynthesis as an example. Methods Mol Biol 1083: 287-311

Lange I, Poirier BC, Herron BK, Lange BM (2015) Comprehensive assessment of transcriptional regulation facilitates metabolic engineering of isoprenoid accumulation in Arabidopsis. Plant Physiol 169: 1595-1606

Lecain E, Chenivesse X, Spagnoli R, Pompon D (1996) Cloning by metabolic interference in yeast and enzymatic characterization of *Arabidopsis thaliana* sterol delta 7-reductase. J Biol Chem 271: 10866-10873

Li F, Asami T, Wu X, Tsang EW, Cutler AJ (2007) A putative hydroxysteroid dehydrogenase involved in regulating plant growth and development. Plant Physiol 145: 87-97

Lovato MA, Hart EA, Segura MJ, Giner JL, Matsuda SP (2000) Functional cloning of an *Arabidopsis thaliana* cDNA encoding cycloeucalenol cycloisomerase. J Biol Chem 275: 13394-13397

Men S, Boutté Y, Ikeda Y, Li X, Palme K, Stierhof YD, Hartmann MA, Moritz T, Grebe M (2008) Sterol-dependent endocytosis mediates post cytokinetic acquisition of PIN2 auxin efflux carrier polarity. Nat Cell Biol 10: 237-244

Meng L and Feldman L (2010) A rapid TRIzol-based two-step method for DNA-free RNA extraction from Arabidopsis siliques and dry seeds. Biotechnol J 5: 183-186

Minami A, Tominaga Y, Furuto A, Kondo M, Kawamura Y, Uemura M (2015) Arabidopsis dynamin-related protein 1E in sphingolipid-enriched plasma membrane domains is associated with the development of freezing tolerance. Plant J 83: 501-514

Moreau RA, Nyström L, Whitaker BD, Winkler-Moser JK, Baer DJ, Gebauer SK, Hicks KB (2018) Phytosterols and their derivatives: structural diversity, distribution, metabolism, analysis, and health-promoting uses. Prog Lipid Res. 70: 35-61

Morikawa T, Mizutani M, Ohta D (2006) Cytochrome P450 subfamily CYP710A genes encode sterol C-22 desaturase in plants. Biochem Soc Trans 34: 1202-1205

Nes WD, Song Z, Dennis AL, Zhou W, Nam J, Miller MB (2003) Biosynthesis of phytosterols. Kinetic mechanism for the enzymatic C-methylation of sterols. J Biol Chem 278: 34505-34516

Pascal S, Taton M, Rahier A (1993) Plant sterol biosynthesis. Identification and characterization of two distinct microsomal oxidative enzymatic systems involved in sterol C4-demethylation. J Biol Chem 268: 11639-11654

Patterson GW, Hugly S, Harrison D (1993) Sterols and phytyl esters of Arabidopsis thaliana under normal and chilling temperatures. Phytochemistry 33: 1381-1383

Qian P, Han B, Forestier E, Hu Z, Gao N, Lu W, Schaller H, Li J, Hou S (2013) Sterols are required for cell-fate commitment and maintenance of the stomatal lineage in Arabidopsis. Plant J 74: 1029-1044

Rahier A, Taton M, Benveniste P (1989) Cycloeucalenol-obtusifoliol isomerase. Structural requirements for transformation and binding of substrates and inhibitors. Eur J Biochem 181: 615-626

Rahier A, Darnet S, Bouvier F, Camara B, Bard M (2006) Molecular and enzymatic characterizations of novel bifunctional 3beta-hydroxysteroid dehydrogenases/C-4 decarboxylases from *Arabidopsis thaliana*. J Biol Chem 281: 27264-2777

Rahier A (2011) Dissecting the sterol C-4 demethylation process in higher plants. From structures and genes to catalytic mechanism. Steroids 76: 340-352

Rasbery JM, Shan H, LeClair RJ, Norman M, Matsuda SP, Bartel B (2007) *Arabidopsis thaliana* squalene epoxidase 1 is essential for root and seed development. J Biol Chem 282: 17002-17013

Rios-Estepa R, Turner GW, Lee JM, Croteau RB, Lange BM (2008) A systems biology approach identifies biochemical mechanisms regulating monoterpenoid essential oil composition in peppermint. Proc Natl Acad Sci USA 105: 2818-2823

Rios-Estepa R, Lange I, Lee JM, Lange BM (2010) Mathematical modeling-guided evaluation of biochemical, developmental, environmental, and genotypic determinants of essential oil composition and yield in peppermint leaves. Plant Physiol 152: 2105-2119

Rondet S, Taton M, Rahier A (1999) Identification, characterization, and partial purification of 4 alpha-carboxysterol-C3-dehydrogenase/ C4-decarboxylase from *Zea mays*. Arch Biochem Biophys 366: 249-260

Schmid M, Davison TS, Henz SR, Pape UJ, Demar M, Vingron M, Schölkopf B, Weigel D, Lohmann JU (2005) A gene expression map of Arabidopsis thaliana development. Nat Genet 37: 501-506

Schrick K, Mayer U, Horrichs A, Kuhnt C, Bellini C, Dangl J, Schmidt J, Jürgens G (2000) FACKEL is a sterol C-14 reductase required for organized cell division and expansion in *Arabidopsis* embryogenesis. Genes Dev 14: 1471-1484

Shan H, Wilson WK, Phillips DR, Bartel B, Matsuda SPT (2008) Trinorlupeol, a major nonsterol triterpenoid in Arabidopsis. Organic Lett. 10: 1897-1900

Shi J, Gonzales RA, Bhattacharyya MK (1996) Identification and characterization of an S-adenosyl-L-methionine: delta 24-sterol-C-methyltransferase cDNA from soybean. J Biol Chem 271: 9384-9389

Souter M, Topping J, Pullen M, Friml J, Palme K, Hackett R, Grierson D, Lindsey K (2002) hydra mutants of Arabidopsis are defective in sterol profiles and auxin and ethylene signaling. Plant Cell 14: 1017-1031

Takahashi D, Imai H, Kawamura Y, Uemura M (2016) Lipid profiles of detergent resistant fractions of the plasma membrane in oat and rye in association with cold acclimation and freezing tolerance. Cryobiol 72: 123-134

582 Taton M, Benveniste P, Rahier A (1989) Microsomal delta 8,14-sterol delta 14-reductase in higher
583 plants. Characterization and inhibition by analogues of a presumptive carbocationic
584 intermediate of the reduction reaction. Eur J Biochem 185: 605-614
585 Taton M, Rahier A (1991a) Properties and structural requirements for substrate specificity of
586 cytochrome P-450-dependent obtusifoliol 14 alpha-demethylase from maize (*Zea mays*)
587 seedlings. Biochem J 277: 483-492
588 Taton M, Rahier A (1991b) Identification of delta 5,7-sterol-delta 7-reductase in higher plant
589 microsomes. Biochem Biophys Res Commun 181: 465-473
590 Taton M, Rahier A. (1996) Plant sterol biosynthesis: identification and characterization of higher
591 plant delta 7-sterol C5(6)-desaturase. Arch Biochem Biophys 325: 279-288
592 Uemura M, Joseph RA, and Steponkus PL (1995) Cold acclimation of Arabidopsis thaliana; effect
593 on plasma membrane lipid composition and freeze-induced lesions. Plant Physiol 109:15-30
594 Vaughan MM, Dorothea Tholl D, Tokuhisa JG (2011) An aeroponic culture system for the study
595 of root herbivory on Arabidopsis thaliana. Plant Methods 7: 5
596 Wewer V, Dombrink I, vom Dorp K, Dörmann P (2011) Quantification of sterol lipids in plants by
597 quadrupole time-of-flight mass spectrometry. J Lipid Res 52: 1039-1054
598 Willemsen V, Friml J, Grebe M, van den Toorn A, Palme K, Scheres B (2003) Cell polarity and PIN
599 protein positioning in Arabidopsis require *STEROL METHYLTRANSFERASE1* function. Plant Cell
600 15: 612-625
601 Zhou W, Nes WD (2003) Sterol methyltransferase2: purification, properties, and inhibition. Arch
602 Biochem Biophys 420: 18-34